APPLIED PHYSICS

Near-UV to mid-IR reflectance imaging spectroscopy of paintings on the macroscale

F. Gabrieli[1]*, K. A. Dooley[1], M. Facini[2], J. K. Delaney[1†]

Broad spectral range reflectance imaging spectroscopy (BR-RIS) from the near UV through the mid–infrared (IR) (350 to 25,000 nm or 28,571 to 400 cm^{-1}) was investigated as an imaging modality to provide maps of organic and inorganic artists' materials in paintings. While visible–to–near-IR (NIR) reflectance and elemental x-ray fluorescence (XRF) imaging spectroscopies have been used for in situ mapping, each method alone is insufficient for robust identification. Combining the two improves results but requires complex data processing. To test BR-RIS, image cubes from early Italian Renaissance illuminated manuscripts were acquired using two spectrometers. Maps of pigments, including trace minerals associated with mined azurite, and their associated binding media were made. BR-RIS has a more straightforward analysis approach as implemented here than visible-to-NIR, mid-IR, or XRF imaging spectroscopy alone and offers the largest amount of macroscale information for mapping artists' materials by comparison.

INTRODUCTION

The use of diffuse reflectance spectroscopy from the near ultraviolet (UV) through the visible and into the near-infrared (NIR) spectral range (350 to 2500 nm or 28,571 to 4000 cm^{-1}) is becoming a routine technique for the in situ characterization of artists' materials either by point analysis (*1*–*3*) or by imaging techniques (*4*–*6*). This spectral range encompasses electronic transitions that give rise to the color of pigments, in addition to overtones and combination bands arising from vibrational modes of chemical bonds mainly involving hydrogen, carbon, nitrogen, and oxygen, including functional groups such as OH, NH, CH, and CO_3. In particular, using high spatial and spectral resolution imaging spectrometers, these characteristic spectral features have been used to identify and map many, but not all, artists' materials including pigments and paint binding media.

To date, mid-IR spectroscopy (mid-IR, 4000 to 400 cm^{-1} or 2500 to 25,000 nm) has been widely used for the successful analysis of microsamples in transmission or reflection mode, as the mid-IR region is rich in spectral features that allow the specific identification of many chemical functional groups contained in artists' materials such as pigments, binders, fillers, and degradation products (*7*). Mid-IR imaging spectroscopy on the microscale has been achieved using attenuated total reflection (ATR) accessories, but this method requires direct contact with a sample from the material under study (*8*, *9*). A limitation to applying mid-IR techniques on the macroscale is that no contact can be made with the artwork. Using noncontact reflectance spectrometers in the mid-IR is fairly challenging for two reasons. First, the no-contact requirement ensures only reflectance mode can be used, and the resulting spectra are more difficult to interpret because they are affected by distortions caused by specular reflections and diffuse reflections within the volume of the material (*10*). In contrast, ATR has very limited penetration into the paint layer, and the measured ATR signal is not distorted by volume scattering. Thus, ATR spectra can be interpreted in a similar way to a transmission spectrum of a thin layer. Second, to acquire sufficient-quality mid-IR reflectance spectra, an IR active source at a temperature much higher than the ambient background is routinely used. These high-temperature sources can heat the painting, which is discouraged for $\Delta T > 5$°C (*11*). Another drawback for doing macroscale mid-IR reflectance imaging spectroscopy is that mid-IR hyperspectral cameras are an order of magnitude more expensive than their visible and NIR counterparts, owing to the higher cost of mid-IR focal plane arrays and imaging spectrometers. For these reasons, macroscale mid-IR reflectance imaging spectroscopy has progressed more slowly than reflectance imaging spectroscopy in the visible and NIR spectral regions.

However, progress has been made in addressing these challenges. Extensive analysis of the distortions in mid-IR spectra has led to an improved capability to assign spectral features to specific vibrational transitions (*10*, *12*). Second, macroscale emissive mode mid-IR imaging spectroscopy has been shown to provide mid-IR spectra that are as good as what can be obtained with mid-IR reflectance mode point spectroscopy without the use of a hot thermal source that risks heating the painting (*13*).

While the mid-IR spectral region is rich in spectral content, the combination of another imaging modality is required for robust identification of artists' materials. Several studies have shown that combining x-ray fluorescence (XRF) elemental mapping with either visible-to-NIR reflectance imaging spectroscopy or mid-IR reflectance or emissive mode imaging spectroscopy yields more robust results (*14*, *15*). However, this requires the combination of two distinctly different image processing methods and algorithms (to handle the elemental and molecular spectroscopic imaging results), which can be challenging and time-consuming. Current methodologies first involve the image registration of the data. Second, molecular maps from the reflectance imaging spectroscopy data that relate to specific pigment or functional groups are made. Element maps are made by fitting the XRF imaging spectroscopic data. The comparison of the maps is often done by visual inspection, but in at least one case, an expert user model was used to automatically refine the material maps by incorporating information derived from the two imaging modalities (*16*), but this is an exception and not the norm.

Instead of performing two modality imaging spectroscopy as discussed above, here we explore the potential of broad spectral

[1]Scientific Research Department, National Gallery of Art, Washington, DC 20565, USA. [2]Paper Conservation Department, National Gallery of Art, Washington, DC 20565, USA.
*Present address: Rijksmuseum, Scientific Research, Hobbemastraat 22, 1071 ZC Amsterdam, Netherlands.
†Corresponding author. Email: j-delaney@nga.gov

range reflectance imaging spectroscopy (BR-RIS) spanning the near-UV to the mid-IR spectral regions (350 to 28,000 nm or 28,571 to 400 cm^{-1}) and a single processing protocol to identify and map a wide range of artists' materials in situ. The approach relies on the rich molecular content that can be obtained from spectral analysis in the visible, NIR, and mid-IR regions related to electronic and vibrational transitions of inorganic and organic functional groups. To test the potential of BR-RIS, we collected three-dimensional (3D) image cubes (2D spatial and 1D spectral) using a simple single-pixel scanner consisting of two point spectrometers and a computer-controlled easel that moved the artwork. One spectrometer covered the spectral range from 28,571 to 4000 cm^{-1} (350 to 2500 nm), and the mid-IR spectrometer covered the spectral range from 5500 to 400 cm^{-1} (1818 to 25,000 nm), providing spectral overlap that was used to scale differences between the spectra. The two image cubes were concatenated and subsequently processed with a convex geometry–based algorithm. Three paintings were analyzed, including a mock-up painting created using modern tube paints, and paintings from illuminated manuscripts, one by Lorenzo Monaco, the *Praying Prophet* (ca. 1410/1413), and another titled *Christ and the Virgin Enthroned with Forty Saints* (ca. 1340) by the Master of the Dominican Effigies.

RESULTS

To test the feasibility of BR-RIS for the identification and mapping of pigments, fillers, and paint binders, we first examined an unvarnished mock-up painting. The mock-up (Fig. 1A) has been previously described and analyzed (*13*). In brief, it was prepared using three sets of commercial tube paints. Each set contained the same primary pigments [phthalocyanine blue, quinacridone red, Hansa yellow, brown earth, cadmium (Cd) red, and zinc (Zn) white] but in a different paint binder (drying oil, acrylic, and alkyd). Paint tubes with the same primary pigment often contained different fillers. The use of each paint, applied in a single layer on the prepared ground, ensured that the mock-up painting contained every pigment/binder combination despite regions with the same primary pigment having a similar visual appearance. A 21 by 11 cm^2 section of the unvarnished mock-up painting was scanned with both spectrometers, and the broad spectral range image cube was constructed as described in Materials and Methods.

First, the ability to map a specific pigment and filler combination was tested. To map the pigment phthalocyanine blue (phthalo blue) (Fig. 1B), we used the spectral range from 700 to 1200 nm, as it contains a broad absorption edge and the narrow absorption feature at 1100 nm (Fig. 1C). As expected, the map shows that all the blue

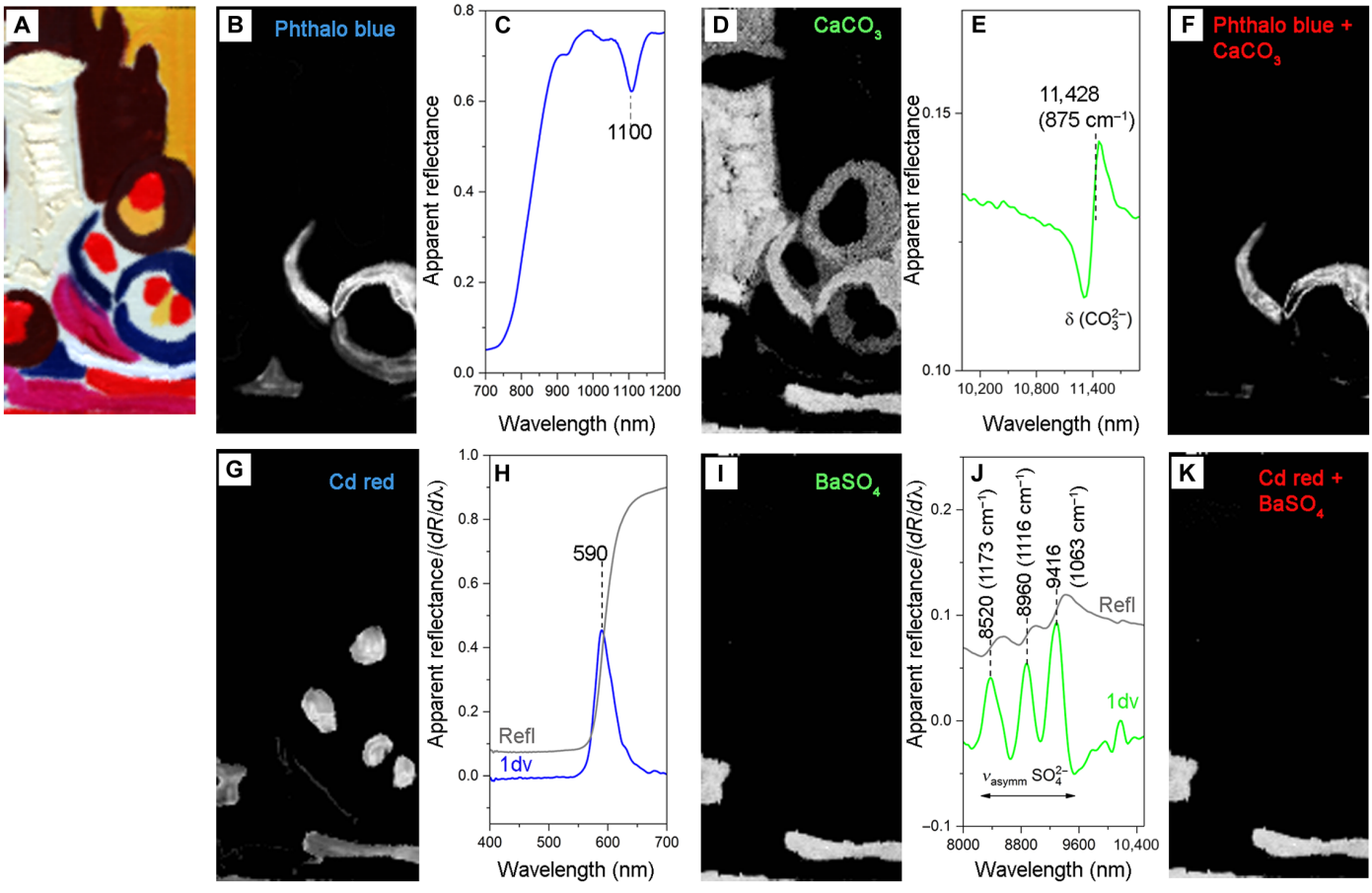

Fig. 1. Mock-up painting: Mapping pigments and fillers. (**A**) Color detail of the mock-up painting. (**B**) Map obtained with the portion of the spectral endmember (**C**) containing the 1100-nm band of phthalo blue. (**D**) Map of the filler $CaCO_3$ obtained from the portion of the mid-IR spectral endmember (**E**). (**F**) Map obtained using the combined spectral portions of the spectral endmember (C and E) used to map the pigment, phthalo blue, and the filler, $CaCO_3$. (**G**) Map obtained with the first derivative of the spectral endmember of the cadmium red pigment (**H**). (**I**) Map of the filler $BaSO_4$ obtained from the first derivative portion of the mid-IR spectral endmember (**J**). (**K**) Map obtained using the combined spectral portions of the endmember used to map the pigment and the filler.

paint contains the pigment phthalo blue. To determine where calcium carbonate ($CaCO_3$) is present, we also mapped the out-of-plane carbonate bending mode at 875 cm^{-1} (11,428 nm) in the mid-IR reflectance spectra, showing a derivative-like distortion (Fig. 1E), using the spectral angle mapper (SAM) algorithm. The $CaCO_3$ map (Fig. 1D) shows that this material is found in some of the blue, white, red, and brown areas. Visually comparing the maps in Fig. 1 (B and D) shows that only the two top arcs of blue paint contain both phthalo blue and $CaCO_3$, likely added as a filler to the tube paint. By combining the reflectance features found in two separate spectral regions (NIR and mid-IR in this case), a single map of phthalo blue and $CaCO_3$ (Fig. 1F) can be made from the BR-RIS image cube using the SAM algorithm.

In a similar way, a map of the red pigment and a filler can be made, although the first derivative of the reflectance image cube with respect to wavelength was used. The first derivative demonstrates the quality of the spectral data acquired and also allows more accurate maps to be obtained as the first derivative spectra accentuate signals of simple transition edges and enhance narrow spectral features present on a broadly varying background (*17*). The reflectance endmember of the red areas (Fig. 1H) shows a steep inflection, and its first derivative spectrum shows a sharp symmetric peak about 40 nm wide (full width at half maximum). This spectral feature is characteristic of an electronic transition from a valence band to a conduction band. The spectra of semiconductor pigments such as vermilion (HgS) or cadmium red (CdS_xSe_{1-x}) display these transitions at 590 nm, since the bandgap of Cd red can be tuned by the amount of Se substituted in for S in the crystal lattice. Here, additional information would be required to distinguish between these two pigments, such as identification of the chemical elements present or the detection of molecular fluorescence from the trap emissions of Cd pigments (*18*). In this case, since this is a mock-up painting, the pigment is known to be Cd red, and the associated map (Fig. 1G) shows all of the red regions to be painted with this pigment, distinct from the deep pink–purple–painted areas.

Barium sulfate ($BaSO_4$), which has a triply degenerate asymmetric stretching mode that gives rise to three distinctive features in the mid-IR fingerprint region and three peaks in the first derivative spectrum (Fig. 1J), was mapped. The associated SAM map of $BaSO_4$, when compared with the Cd red map, shows that it is present in only two regions of the Cd red paint (Fig. 1I). Using the combined reflectance spectra of the Cd red pigment and $BaSO_4$, a SAM-derived map confirms this observation (Fig. 1K). Comparing this joint map with that of the $CaCO_3$ map in Fig. 1D shows that the Cd red pigment with $BaSO_4$ also contains $CaCO_3$. These examples demonstrate the use of BR-RIS for the identification and mapping of pigments, fillers, and paint binders on a mock-up painting with a simple layer structure.

To test the capability of BR-RIS to map the three paint binders in the mock-up painting, the same analysis procedure was performed on discrete spectral ranges in the NIR [6250 to 4000 cm^{-1} (1600 to 2500 nm)] and mid-IR [1800 to 1100 cm^{-1} (5555 to 9009 nm)]. These regions are rich with vibrational transitions associated with C═O, C─C, C─O, C─O─C, and C─H functional groups that are useful for the identification of historic paint binders such as drying oils, gums, and egg tempera, and modern binders such as alkyds and acrylics (*2*, *10*, *12*). In separate studies, the use of each spectral region to map these binders was demonstrated (*11*, *17*). While the mid-IR region encompasses many distinct vibrations due to the presence of binding media, the region also suffers from spectral interference from vibrations of some common inorganic pigments, such as those containing carbonate groups. The absorption bands present in the NIR region are narrower and suffer less from pigment interference but are weaker. Thus, processing both spectral regions can help remedy this problem.

Because mapping oil and alkyd paint binders has been demonstrated using NIR spectral features (*17*), the example here focuses on the added use of the mid-IR portion of the reflectance image cube (Fig. 2E) to identify and map the three binders used for the mock-up painting (drying oil, alkyd, and acrylic). The key features for the identification of drying oil were the carbonyl stretch (C═O) at ~1740 cm^{-1} (~5747 nm) and the C─H bending at ~1450 cm^{-1} (~6896 nm). An alkyd binder, which is a polyester modified by the addition of fatty acids, shares spectral features with an oil binder, but the alkyd was identified and mapped using the additional C─O─C stretching present at ~1270 cm^{-1} (~7874 nm). Last, the acrylic binder was identified by C─C stretching at ~1175 cm^{-1} (8510 nm) and the sharp shape of the C═O feature at ~1740 cm^{-1}

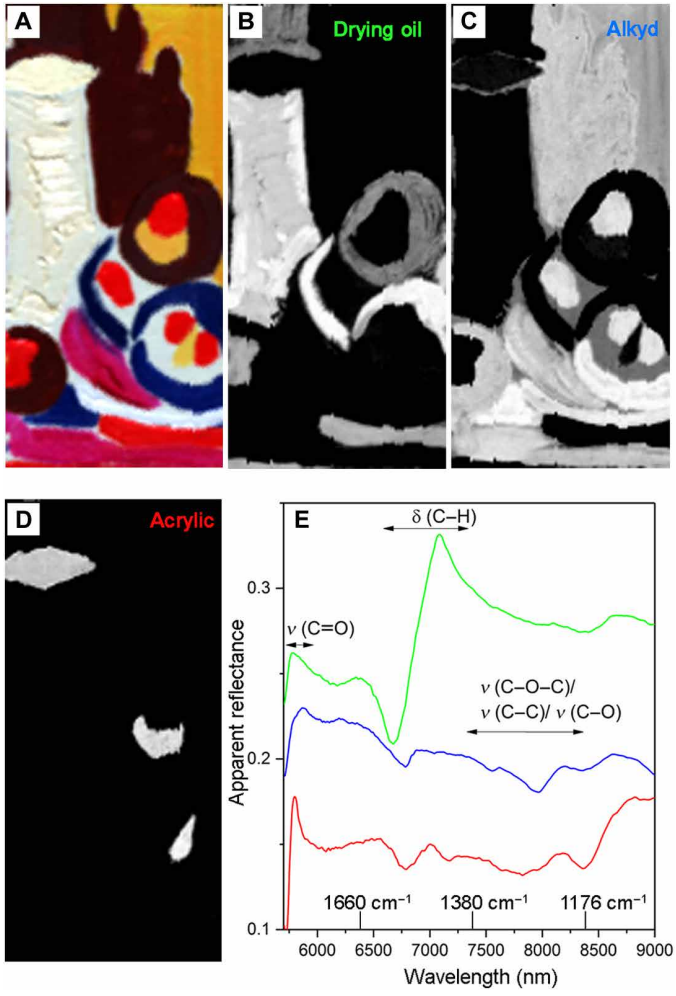

Fig. 2. Mock-up painting: Mapping binders. (**A**) Color detail of the mock-up painting. (**B** to **D**) Maps of drying oil (green), alkyd (blue), and acrylic (red) binders obtained from using the spectral endmembers shown in the graph (**E**) obtained from the BR-RIS spectral image cube.

(~5747 nm). The binder distributions in the resulting maps are consistent with where the binders were known to be used.

As shown in Fig. 2 (B to D), drying oil was used for some of the brown, white, blue, and red paints for the detail of the mock-up painting shown. Alkyd was used for portions of the white and yellow paints, and acrylic was used for some of the brown, blue, red, yellow, and deep pink–purple paints, in addition to the white ground. Comparison of the binder maps with those of the pigments and fillers (Fig. 1) allows some observations about the compositions of the commercial paints to be made. Two different paint formulations were used for the blue areas shown. The phthalo blue– and $CaCO_3$-containing paint (Fig. 1F) was associated with drying oil, whereas the phthalo blue paint in which no $CaCO_3$ was detected was painted in an acrylic binder. For the red areas containing Cd red, $BaSO_4$, and $CaCO_3$, a drying oil was used. The rest of the red areas were painted with Cd red pigment in an acrylic binder. While these are only a subset of the results obtained, they demonstrate the potential of BR-RIS to successfully identify and map many key artists' materials with the SAM algorithm.

To test the suitability of BR-RIS on actual historical artworks, we analyzed two illuminated manuscript paintings on parchment from large choir books made during the 14th and 15th centuries of the Italian Renaissance. Illuminated manuscripts were chosen as test cases because they are unvarnished and contain artist materials typically found in paintings from this time period. While illuminated manuscript paintings often have a simple paint layer structure compared to a painting, the artworks chosen here contain complex stratigraphy similar to that found in panel paintings by the same artists. For example, the layering of red lake glazes on top of vermilion was used to create shading and the illusion of depth. Another key advantage is that the pigments used in these works have already been identified and mapped.

The *Praying Prophet* (ca. 1410/1413) (Fig. 3A) is from the choir book known as codex H74 that was painted by Lorenzo Monaco and his workshop for the church of S. Egidio in the Hospital of Santa Maria Nuova. This choir book is one in a series commissioned by the Camaldolese monks of Santa Maria degli Angeli in Florence. The painting shows a hooded prophet in prayer inside the initial E with surrounding foliage marginalia. The *Praying Prophet* painting has been studied previously, and a map of the pigments was made (*19*). Of particular interest was the finding that the figure of the prophet was painted with an egg yolk tempera paint binder (*20*). The identification and mapping of the egg yolk tempera were done with NIR reflectance imaging spectroscopy using the CH_2 combination band in the region of 4350 to 4325 cm^{-1} (2300 to 2313 nm), which is associated with lipid. The wavelength position of this lipidic band can be used to discriminate between a drying oil (2304 nm), egg yolk (2309 nm), or wax (2312 nm). While spectral features associated with protein [4902 and 4598 cm^{-1} (2040 and 2175 nm) related to the C═O, N─H, and C─N functional groups] can be seen in the NIR, they cannot be solely attributed to the binder as the NIR light penetrates through the paint layers to the protein-rich parchment. Thus, the NIR spectral region could not be used to confirm the protein component of egg yolk. Studies of the other paintings in codex

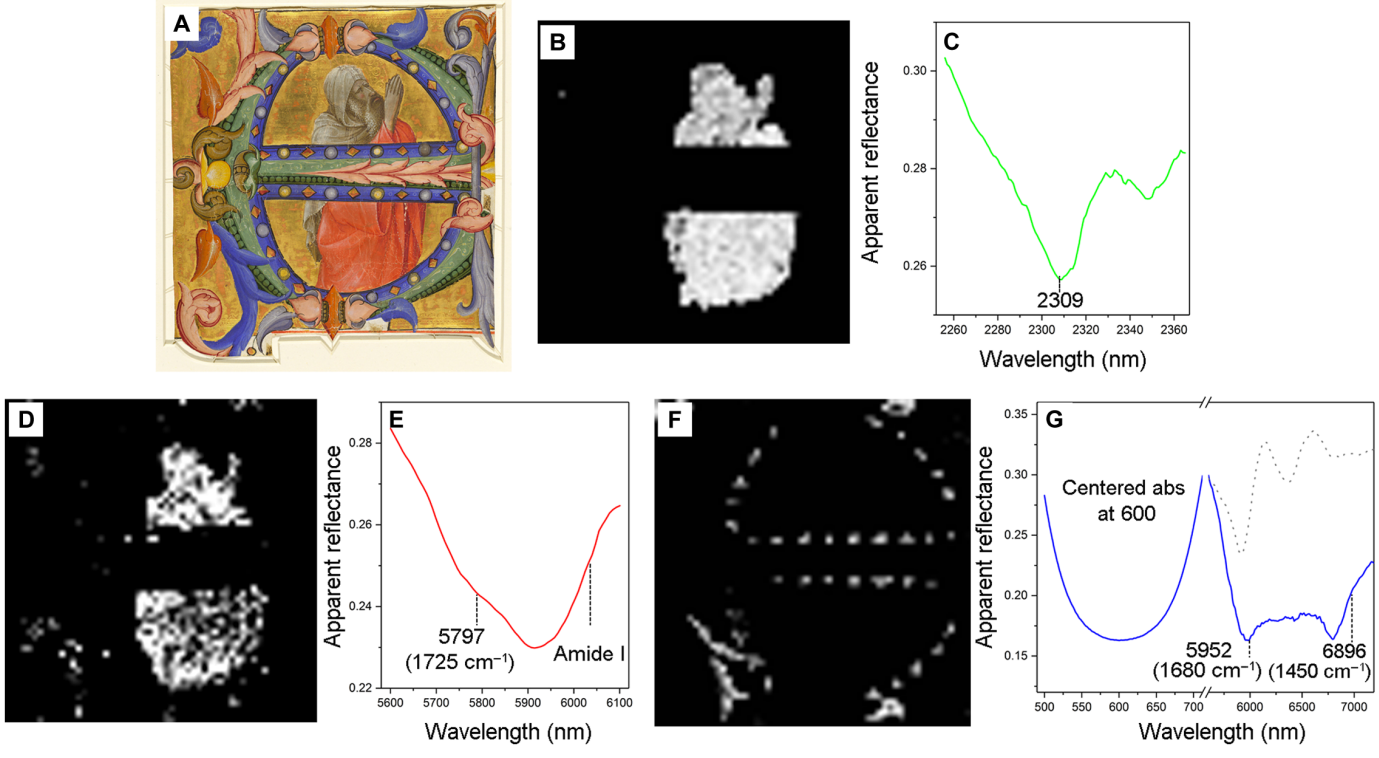

Fig. 3. *Praying Prophet* by Lorenzo Monaco: Mapping binders. (**A**) Color image of Lorenzo Monaco's *Praying Prophet* (ca. 1410/1413), Rosenwald Collection, National Gallery of Art. (**B**) Map of the C─H lipidic spectral feature associated with egg yolk (**C**). (**D**) Map of carbonyl group (C═O) spectral features (**E**) associated with the proteic (amide I) and lipidic component (5797 nm or 1725 cm^{-1}) in egg yolk. (**F**) Map of ultramarine and polysaccharide spectral features (**G**) associated with the blue portions of the initial E and blue areas of the marginalia.

H74 also had their central figures painted in egg yolk tempera (*21*). This was an unexpected find because the most widely used paint binding media for miniature paintings on parchment were reported not to be egg yolk tempera but rather protein-based media (animal skin glue and egg white) or polysaccharide-based media (such as gums). In this time period, master painters trained in the guild of doctors and apothecaries normally used egg tempera as a binding medium when painting on panels and murals, and Lorenzo Monaco was trained as a panel painter, so the finding that Monaco likely used egg tempera paint on parchment is perhaps logical. The BR-RIS data were collected in this study on the same manuscript because the limited penetration depth of the mid-IR, compared with the NIR, can enable detection of the binding media without contribution of the parchment. The mid-IR portion of the spectra can be used to confirm the presence of egg yolk tempera in the central figure and also help determine the binders used for the initial E and the foliage marginalia that were not able to be identified with the NIR spectra. With the BR-RIS data, the same CH_2 combination band near 4331 cm^{-1} (2309 nm) mapped in the prior study was used to make a new map, again showing this lipidic spectral feature maps to the central figure of the prophet (Fig. 3, B and C). To confirm the presence of egg yolk, the mid-IR fingerprint region was examined where protein and lipid have two distinguishable C═O stretching vibrations, one related to the lipid component around 1740 cm^{-1} and one included in the amide I of the protein component around 1650 cm^{-1}. The spectral endmember in Fig. 3E shows the presence of C═O stretching associated with lipid content that appears as a shoulder on the protein amide I band. The location of the shoulder at ~1725 cm^{-1} (~5797 nm) and the presence of amide I (showing derivative-like distortion) at ~1660 cm^{-1} (~6024 nm) are consistent with the presence of a lipidic and proteic component as expected for egg yolk. These spectral features map to the figure of the prophet including his white cloak and hood, red robe, head, and arms (Fig. 3D) and confirm the prior study's finding that egg yolk tempera was used to paint the central figure of the prophet.

Further examination of the mid-IR spectral region of the image cube provided evidence of the use of a polysaccharide binder (likely gum) in the blue areas of the initial and marginalia. The blue areas of the marginalia and letter had previously been identified as ultramarine (*19*). The map (Fig. 3F) obtained from the BR-RIS spectral endmember (Fig. 3G) has a strong absorption at 600 nm, typical of ultramarine in the visible, and two features in the mid-IR consistent with vibrational modes of a polysaccharide. For example, in gum arabic, the C═O stretch and intramolecular water feature occurs at 1665 cm^{-1}, which is observed here at ~1680 cm^{-1} (~5952 nm), and the δCH, νC─O, and δCOH bands observed at 1445 cm^{-1} in gum arabic are found here as derivative bands at ~1450 cm^{-1} (~6896 nm) (*22*). No amide features (gray trace in graph Fig. 3G) are observed, thus ruling out the presence of a protein binder. The mid-IR spectral features indicate that a polysaccharide, possibly gum arabic, was used as a binder for the ultramarine. The BR-RIS was also used to confirm that the ultramarine was from a natural mineral source. Natural ultramarine (ideal chemical formula $Na_{7.5}[Al_6Si_6O_{24}]S_{4.5}$) is a mineral structurally organized in B-sodalite cages, in which carbon dioxide (CO_2) may be encapsulated (*23*). Studies of various sources of natural ultramarine, including those likely to be used here, have observed the presence of asymmetric stretching at 2340 cm^{-1}, which is indicative of CO_2 (*23*, *24*). Using the BR-RIS cube, it was possible to map the ultramarine absorbance in the visible range together with the asymmetrical stretching of the CO_2, confirming that all the blue areas consist of natural ultramarine.

In the artwork from the early Italian Renaissance, calcium carbonate was used as a substrate to create insoluble pigments referred to as "lakes," rather than being added as extenders or fillers, as is common in modern paints. Lake pigments are typically valued for their transparent quality and are often mixed or applied as a glaze on top of more opaque colors. From the previous study (*19*), an organic lake pigment was identified in several areas. A pinkish-colored lake was found in the marginalia (with some gypsum present) along with a deep red–colored lake in the dark lowlights on the vermilion robe of the prophet. A yellow lake was found as the pigment used in the yellow leaf of the marginalia, as well as with blue azurite in the initial to create the dark and light green colors. Studies have found that, in general, alkali solutions often made from lime or calcium carbonate were used to make lake yellow and pinkish colorants, whereas alumina salts, such as potassium alum, were used as the substrate to make red lakes (*25*).

From the BR-RIS data, a map of where the calcium carbonate spectral feature at 875 cm^{-1} (11,428 nm) is present is shown in Fig. 4B. These areas map to the pink, yellow, and green in the marginalia. The rest of the maps and endmember spectra in Fig. 4 (C to H) represent the separate lake pigments associated with $CaCO_3$. The pinkish lake of the marginalia (Fig. 4C) has spectra from the BR-RIS cube with two absorption bands near 525 and 560 nm, characteristic of the $\pi \rightarrow \pi^*$ electronic transition seen in reference visible reflectance spectra of insect-based red lake pigments (*26*, *27*) and appearing as peaks in the first derivative spectra at 540 and 589 nm (Fig. 4D). The spectrum in Fig. 4D also shows that the area of the pink lake marginalia contains $CaCO_3$, as evidenced from the 875 cm^{-1} (11,428 nm) feature. The colocalization of the pink lake and $CaCO_3$ suggests that $CaCO_3$ was used as a substrate for the pink lake. Prior analysis of the pink lakes by point XRF had found Ca and, from NIR diffuse reflectance spectra, gypsum, a hydrated calcium sulfate, had been identified from small absorption features near ~6890 to 6450 cm^{-1} (~1450 to 1550 nm) due to the first overtone of OH stretching. The mid-IR spectra were important in determining that gypsum was not the only source of Ca present in the pink lakes. The prior XRF point analysis also found K and trace Al in addition to the Ca. While this finding is still consistent with $CaCO_3$ being used as the substrate for the pink lake, given the prior research noted above (*25*), the detection of trace Al means the use of an aluminum substrate cannot be ruled out.

The first derivative reflectance spectral endmember shown in Fig. 4F represents yellow lake and also $CaCO_3$ (875 cm^{-1} or 11,438 nm). This endmember maps to the yellow marginalia (Fig. 4E). The endmember shown in Fig. 4H represents the pigment azurite and $CaCO_3$. The pigment azurite, a blue hydrated copper-based carbonate $Cu_3(CO_3)_2(OH)_2$, can be determined with certainty from the reflectance spectrum. Specifically, the broad absorbance from ~525 to 900 nm in the visible, an absorbance feature at 6684 cm^{-1} (1496 nm) associated with the first overtone of OH stretching, and additional features at 4376 and 4251 cm^{-1} (2285 and 2352 nm) associated with OH and carbonate group overtone and combination bands are characteristic of the pigment. The CO_3^{2-} bending in azurite occurs at 837 and 817 cm^{-1}, which is shifted relative to CO_3^{2-} bending in $CaCO_3$ at 875 cm^{-1}. This endmember maps to the green marginalia (Fig. 4G), suggesting that azurite was used in conjunction with a yellow lake to create the green color. The colocalization of $CaCO_3$ in

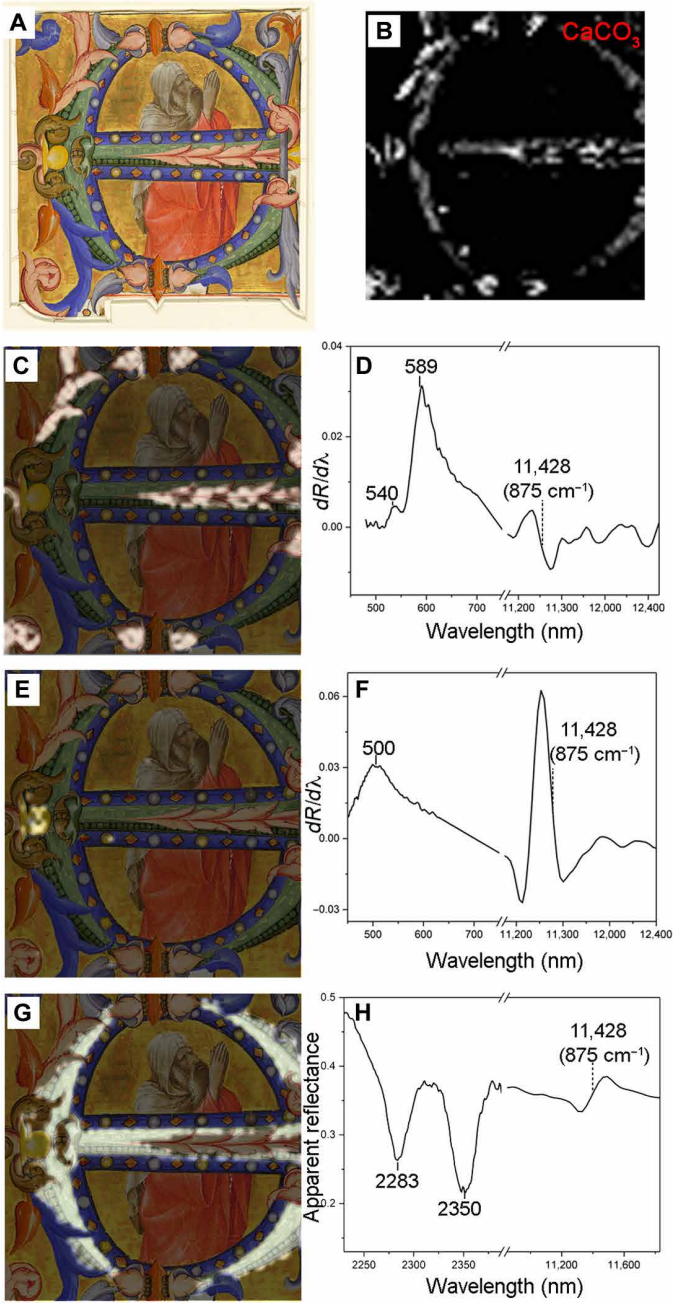

Fig. 4. *Praying Prophet* by Lorenzo Monaco: Mapping lake pigments and associated substrate. (**A**) Color image of the *Praying Prophet*. (**B**) $CaCO_3$ map. (**C**) Overlay of the map obtained from the spectral features of the pink lake and $CaCO_3$ (**D**). (**E**) Overlay of the map obtained from the spectral features of the yellow lake and $CaCO_3$ (**F**). (**G**) Overlay of the map obtained from the spectral features of the yellow lake, azurite, and $CaCO_3$ (**H**).

the green marginalia also suggests that $CaCO_3$ was used as a substrate for the yellow lake. These findings are consistent with the less definitive prior observations by XRF point analysis, which found a small amount of Ca in the yellow and green areas. Thus, there is strong evidence to support that the yellow colorant was laked onto $CaCO_3$.

In the case of the red lake found on the dark folds of the red vermilion robe of the prophet, no spectral evidence in the BR-RIS cube for $CaCO_3$ was found. This is as expected considering that Kirby *et al.* (*25*) found that it was more common for alumina salts, such as potassium alum, to be used as substrates for red lakes. Prior XRF point analysis of the dark red folds in the robe found no Ca but did find K and trace Al, consistent with the hypothesis that the substrate for the red lake is likely potassium alum. Unfortunately, no evidence of potassium alum (potassium aluminum sulfate) was found in the BR-RIS spectrum, either through the presence of sulfate stretches or Al—O vibrations. While in the micro–FTIR (Fourier transform IR) spectroscopy of the samples, the Al—O vibration and sulfate stretch have been observed on an isolated layer or particles (*25*), in the reflectance mode, these vibrations are hard to observe because of the interference with components in the paint layers.

The manuscript painting of *Christ and the Virgin Enthroned with Forty Saints* (ca. 1340) is from the famed *Laudario of Sant'Agnese*, a choir book commissioned sometime around 1340 by a Laudesi confraternity of local men and women who gathered regularly to sing hymns to the Virgin Mary and her fellow saints in the Celestial Paradise. The book commemorates temporal feasts in the liturgical year and consists of paintings and songs written by these lay singers in the Italian vernacular, rather than Latin. The book was of very high quality, representing the wealth of this confraternity that met in the Carmelite church of Santa Maria del Carmine in Florence. The book was illuminated by two master painters, Pacino di Bonaguida and an unknown artist identified only as the Master of the Dominican Effigies. The painting examined here is attributed to the latter artist. This illumination has been previously studied, and the pigments were identified and mapped (*23*).

The areas of the blue sky and the robes of Christ and Mary appear darker in tone than the lighter blue areas such as the saints' robes. All of these regions were found in the prior study to have been painted with the blue mineral azurite by using reflectance imaging spectroscopy and near-UV–to–NIR point reflectance spectroscopy (*28*). Prior point XRF analysis discovered differences in the types of trace elements found between the darker and lighter blue areas. The darker areas of azurite contained traces of arsenic (As) and bismuth (Bi) and a small amount of zinc (Zn), whereas the lighter blue areas contained only Zn but in a relatively larger amount.

The identification and characterization of elemental impurities are important, as this gives additional information about the mineral source. Azurite and malachite, both copper carbonate hydroxides, are the most common Cu-based minerals used as pigments, but in nature, many other Cu-based hydrated carbonates coexist in minor quantities, such as rosasite $(Cu,Zn)_2(CO_3)(OH)_2$, in which Zn substitutes for Cu in the crystal lattice, resulting in a light green color. The presence of rosasite has been previously inferred from elemental information in azurite paint layers of Italian Renaissance paintings (*29*, *30*). Other impurities in azurite and malachite can include smithsonite, which is a white zinc carbonate ($ZnCO_3$), or mixite, which is a green bismuth (Bi)– and arsenic (As)–containing copper mineral $[BiCu_6(AsO_4)_3(OH)_6{\cdot}3(H_2O)]$ identified and confirmed by Berrie *et al.* (*31*) in the azurite paint layer of the robe of the Madonna in Giotto's panel painting *Madonna and Child* (ca. 1310/1315).

Smieska *et al.* (*32*) showed that maps of trace elements in paintings and marginalia of illuminated manuscripts could be obtained with a bright synchrotron x-ray source and a high-speed detector. Thus, XRF imaging spectroscopy could confirm the point analysis hypothesis that two different sources of azurite were used as inferred from the differences in the trace elements. Using the Gallery's in-house

XRF scanner, a 5.6 by 2.4 cm^2 detail of *Christ and the Virgin Enthroned with Forty Saints* was scanned, and the resulting elemental maps for Zn (Fig. 5D) and As (Fig. 5E) confirm the results from the XRF point analysis. Zn is found in the light blue robe of the saint and is also found in lesser quantity in the dark blue sky. As and Bi (map not shown) occur only in the dark blue azurite sky. The detection of As and Bi suggests the presence of mixite, but to confirm this assignment requires chemical structure information either from x-ray diffraction (XRD) or vibrational spectroscopy. Since sampling was prohibited for this work on parchment, in situ methods were required. An in situ method has been recently adapted for making XRD maps of works of art (*33*), but given the low abundance of the mineral in the concentrated field of azurite, XRD mapping was expected to be challenging. Instead, we sought to determine whether BR-RIS could be used for the identification and mapping of functional groups characteristic of trace minerals.

The mid-IR reflectance spectrum of azurite is well known and highly specific of the mineral due to the CO_3^{2-} asymmetric and symmetric stretching at 1490 to 1415 cm^{-1} and 1091 cm^{-1}, CO_3^{2-} bending at 837 and 817 cm^{-1} (and their combination bands in the region 2450 to 2600 cm^{-1}), and OH stretching at 3425 cm^{-1} (Fig. 5G, "Azurite std") (*10*, *34*). The mid-IR spectrum of rosasite shows vibrational modes related to the asymmetric and symmetric stretching of the carbonate group (1488, 1388, and 1096 cm^{-1}), bending of the carbonate group (870 and 818 cm^{-1}), a strong bending of the OH group (1047 cm^{-1}), and two characteristic OH stretches at ~3250 and 3500 cm^{-1} (*35*). The smithsonite ($ZnCO_3$) mid-IR spectrum shows vibrational modes at 1408, 1085, 876, and 743 cm^{-1} for asymmetric stretching, symmetric stretching, in-plane bending, and out-of-plane bending, respectively (*36*), that are slightly shifted with respect to azurite or calcium carbonate absorption bands. Because of this near overlap, the detection of smithsonite in the presence of azurite is challenging when reflectance mid-IR spectroscopy is used. Arsenate-based minerals have characteristic mid-IR absorptions related to asymmetric stretching of the arsenate group (AsO_4^{3-}) at ~820 cm^{-1} and As—OH in-plane and out-of-plane bending, clearly visible in the mid-IR reflectance spectrum of a mixite reference sample at 1165 and 550 cm^{-1} (Fig. 5G, "Mixite std") (*37*).

BR-RIS was completed in the same region previously analyzed with XRF imaging spectroscopy. As expected, azurite was detected in both the dark and lighter blue areas using the visible and NIR spectral features (Fig. 5H) of the reflectance spectra associated with azurite. Examination of the mid-IR portion of the BR-RIS cube in the spectral range where features of zinc-containing rosasite or smithsonite occur provided no evidence for either mineral, although the presence of smithsonite cannot be ruled out because of its spectral overlap with azurite.

The examination did reveal spectral features characteristic of the arsenate bending and stretching characteristic of mixite, specifically the As—OH bending mode at 1165 cm^{-1} (8584 nm). When the

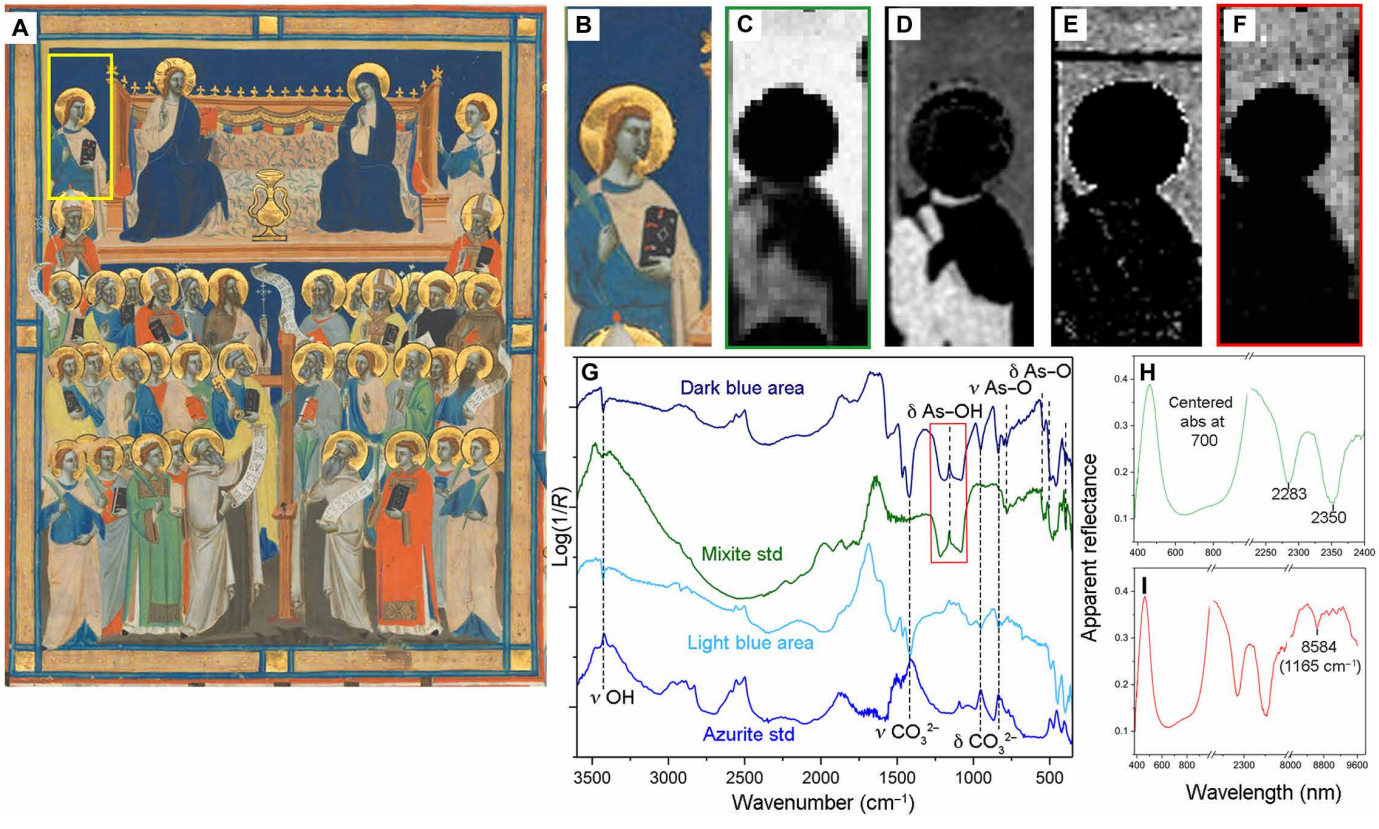

Fig. 5. *Christ and the Virgin Enthroned with Forty Saints*: Identification and mapping of azurite and mixite in blue areas. (**A**) Color image of the Master of the Dominican Effigies' *Christ and the Virgin Enthroned with Forty Saints* (ca. 1340), Rosenwald Collection, National Gallery of Art. (**B**) Color detail studied. (**C**) Map of azurite obtained from the reflectance spectrum (**H**). (**D**) Elemental map of zinc (Kα). (**E**) Elemental map of As (Kβ). (**F**) Map of the As—OH reflectance feature attributed to mixite and the spectral features of azurite in visible and NIR (**I**). (**G**) Mid-IR reflectance spectra of the dark blue and light blue areas, in addition to mixite and azurite standards.

As—OH spectral feature and that for azurite is used to make a map, only the areas of dark azurite are highlighted (Fig. 5F). Thus, mixite is present throughout the entirety of the sky background.

DISCUSSION

The object of the research was to explore the suitability of BR-RIS as an in situ tool for the identification and mapping of many organic and inorganic materials used in fine art paintings. Of particular interest was the desire to use the same set of image processing tools to merge the spectral information contained in the visible, NIR, and mid-IR spectral regions, which includes electronic transitions, fundamental vibrational transitions, and their associated overtone and combination bands. The case studies of a reference mock-up painting and two historic illuminated manuscripts show the potential of this data collection and analysis methodology to identify and map pigments, paint binders, fillers, and substrates used for lake pigments.

The success of the proposed methodology comes, in part, because of the rich literature within the cultural heritage community as well as the geophysical community about the identification of a wide variety of pigments, many of which are natural minerals. Of special importance are the studies that have interpreted the mid-IR reflectance spectra, which contain distortions by the specular reflections within the sample volume that are not seen in transmitted mid-IR spectra due to the thin sample layer required. Last, while more advanced analysis tools exist than those used here, the SAM and matched filter algorithms used proved suitable for the analysis of the datasets. That said, the collection of broad spectral range image cubes on a large number of artworks would be ripe for new machine learning algorithms.

Despite the successes here, there is one key aspect that limits a wider adoption of the proposed approach: the scan rate (area scanned per unit time). In the system demonstrated here, the scan rates were 0.2 to 1 mm/s for a spatial sampling of 1 to 2 mm^2. Scanning a 1-m^2 painting at 1-mm^2 sampling at 0.2 mm/s would take several months. Two methods could be used to increase the scan rate, either by decreasing the integration time for single-pixel scanners or multiplexing by increasing the number of spatial pixels collected at the same time from 1 pixel to hundreds. Getting to scan rates of 10 mm/s for 1-mm^2 sampling is achievable in the near-UV–NIR, but more work needs to be done to achieve these rates in the mid-IR, perhaps by using broadband mid-IR laser sources. This would result in ~30 hours to scan a 1-m^2 painting, which is comparable to XRF scanners having high-quality spectra (*15*, *38*). Multiplexing the number of pixels across the spectrometer slit is also possible and would require using imaging spectrometers rather than point scanners. Imaging spectrometers from the visible to the mid-IR exist, with scan rates of 1 m^2/hour or less at a spatial sampling of 1 mm^2 at illumination conditions suitable for paintings. Commercial imaging systems operating at these rates in the visible to NIR now exist. Hyperspectral cameras also exist for portions of the mid-IR, and we have used a high-throughput low-noise mid-IR camera operating from 1240 to 760 cm^{-1} to collect image cubes of paintings at room temperature in emissive mode at scan rates of 0.5 m^2/min at 1-mm^2 spatial sampling (*13*). However, the drawbacks of commercial mid-IR imaging systems include the much higher costs due to increased complexity of the spectrometer and the mid-IR focal planes. They also do not currently provide the needed sensitivity.

The other challenge is the paint system itself, which consists of either pure or intimately mixed pigments in thin layers of paint typically a few to tens of micrometers thick over a ground preparation. The paint layers can be as few in number as one to tens of layers; however, typically, only a few layers are present. Given that the pigment particles vary from submicrometers to ~5 micrometers in size, effects of light scattering in these thin layers play a role. The implications are that the penetration depth of the light changes from the visible (limited penetration) to the NIR (penetration often to the ground layer of the painting) to the mid-IR (limited penetration). The effect of this needs to be considered in the interpretation of the spectral features observed in each portion of the spectra. Other practical limitations need to be considered such as the impact of the varnish layer; however, this is not an issue for illuminated manuscripts since they are unvarnished. While varnish layers are mostly transparent in the visible and NIR and contribute negligibly to the reflectance spectra in these regions, it can dominate the spectral features present in mid-IR spectra. Thus, the proposed methodology is best suited for unvarnished paintings or for use when paintings are undergoing treatment to remove aged and discolored varnish. It is during this time that paintings typically are studied in great detail, making this possible drawback less of a problem. Last, while BR-RIS provides a large amount of information on organic and inorganic materials, not all materials can be conclusively identified with these spectral regions. Elemental information will continue to aid in the robust identification and mapping of artists' materials.

Specific questions of interest in cultural heritage science that BR-RIS could address given the results here include identifying and mapping the distribution of pigments and associated extenders in commercial tube paints. This could be useful in cases where specific brands of tube paint were known to have been used by particular artists. For example, a rich correspondence between Vincent van Gogh and his brother Theo is well documented and has been related to compositional analysis of paint tubes contemporary to van Gogh. BR-RIS image cubes appear to offer the largest amount of macroscale information for mapping artists' materials with a more straightforward analysis approach than visible-to-NIR, mid-IR, or XRF imaging spectroscopy alone.

MATERIALS AND METHODS

The broad spectral range image cubes were collected using a computer-controlled easel to move the artwork (SatScan System, LG Motion, UK) (*39*) and two separate, stationary spectrophotometers, each covering a different portion of the total spectral range. The UV to NIR spectral range (28,571 to 4000 cm^{-1} or 350 to 2500 nm) was collected using an optical fiber spectrometer, and the mid-IR range (5500 to 400 cm^{-1} or 1818 to 25,000 nm) was covered using an FTIR spectrometer. The data from each spectrometer were converted to apparent reflectance using known reflectance standards. The positional information from the easel controller was used in concatenating the two spectral image cubes together. The same spatial collection step size was used for both spectrometers. A spatial sampling of 1 mm was used for the mock-up painting and the detail of the illuminated manuscript by the Master of the Dominican Effigies, and 2 mm for the manuscript by Lorenzo Monaco. Since different integration times were needed for each spectrometer to ensure high-quality spectra, the image cube collections with each spectrometer were not collected concurrently.

Near-UV to NIR scanning

The experimental details for single-pixel scanning of paintings using a fiber spectrometer (ASD FS3; Malvern Panalytical) were described before (*34*). A scan rate of 1.3 mm/s was used to collect the data with a spatial response function of 2 mm^2. A fiber optic halogen lamp (30-W fiber optic illuminator, Malvern Panalytical) was used to illuminate a ~3-mm-diameter spot at 3000 lux. To improve the quality of the reflectance spectra in the 7692 to 4000 cm^{-1} (1300 to 2500 nm) spectral region, a supplemental halogen light source (Leaf probe, Malvern Panalytical) with a 1350-nm cut-on long-pass filter (Edmund Optics) was used. The fiber probe was normal to the painting surface, and both illumination sources, although offset from each other, were at ~45° from the painting normal. The integration time used during the scan was 68 ms with four averages for each acquisition. The spectral sampling was 1.4 nm from 350 to 1000 nm and 1.1 nm from 1000 to 2500 nm.

Mid-IR scanning

A point FTIR spectrometer (ALPHA, Bruker) operating in standoff reflectance mode was used to collect reflectance spectra from ~5500 to 400 cm^{-1} (1818 to 25,000 nm), thus providing overlap with the spectra from the UV to NIR spectrometer. The measured spatial response function of the spectrometer in this mode is 1.5 mm^2, and the area illuminated is 4 by 5 mm. The spectral sampling was 4 cm^{-1}, which matches the NIR portion of the other spectrometer. The effective integration time required to obtain good-quality spectra was the time to collect three spectra, about 5 s. Given this long collection time, the scanning easel was operated in a stop and stare mode, that is, it moved to a predetermined position using the easel linear encoders, and the spectrum was collected before moving to the next position.

Using the positional information from the easel, the reflectance spectra collected from each spectrometer were assembled into an image cube. The UV-NIR image cube had 2151 spectral bands, and the mid-IR cube had 3468 bands. Given that the solid angles are different between the two spectrometers, the mid-IR reflectance spectra were scaled to match the spectral offset of the corresponding UV-NIR reflectance spectra using the common NIR region (5500 to 4000 cm^{-1} or 1818 to 2500 nm) shared by the two spectrometers. The two cubes were then concatenated to form a single image cube for further processing given that they were acquired with the same spatial sampling as noted above.

The exploitation of the resulting single image cube was done using the spectral analysis tools contained in the ENVI (Harris Corp.) remote sensing software package. Spectral endmembers, reflectance spectra representing specific materials, were identified by manually looking for known spectral features of the chemical compounds of interest in the image cube. The SAM or the mixture tuned matched filter algorithms were used to make maps of the materials of interest. To enhance the quality of the maps, only portions of the reflectance spectral endmembers with characteristic spectral features were used in the image processing. An internal spectral library and published spectral information about the artists' materials of interest were used in the spectral assignments.

XRF scanning

XRF data were collected using a self-constructed XRF imaging spectrometer in which the easel was used to scan a detail of the painting titled *Christ and the Virgin Enthroned with Forty Saints*. The x-ray source consisted of a rhodium 50-W tube, operated at 50 kV and 0.75 mA, with a converging capillary optic that gave a spot size of 0.5-mm diameter at the work of art. A solid-state XRF detector was used (Vortex, Hitachi) with a 50-mm^2 detector area with a 1-μs peaking time and an integration time of 2 s. The positional information from the easel was used to reconstruct the XRF cube, and elemental maps were made using an in-house software tool that fits Gaussians to the detected peaks (*16*). The integrated area from the peak-fitting procedure is displayed in the specified maps for each element's emission line.

REFERENCES AND NOTES

1. M. Picollo, M. Bacci, A. Casini, F. Lotti, S. Porcinai, B. Radicati, L. Stefani, Fiber optics reflectance spectroscopy: A non-destructive technique for the analysis of works of art, in *Optical Sensors and Microsystems* (Springer, 2002), pp. 259–265.
2. M. Vagnini, C. Miliani, L. Cartechini, P. Rocchi, B. G. Brunetti, A. Sgamellotti, FT-NIR spectroscopy for non-invasive identification of natural polymers and resins in easel paintings. *Anal. Bioanal. Chem.* **395**, 2107–2118 (2009).
3. M. Aceto, A. Agostino, G. Fenoglio, A. Idone, M. Gulmini, M. Picollo, P. Ricciardi, J. K. Delaney, Characterisation of colourants on illuminated manuscripts by portable fibre optic UV-visible-NIR reflectance spectrophotometry. *Anal. Methods* **6**, 1488–1500 (2014).
4. J. K. Delaney, J. G. Zeibel, M. Thoury, R. O. Y. Littleton, M. Palmer, K. M. Morales, E. R. de la Rie, A. N. N. Hoenigswald, Visible and infrared imaging spectroscopy of Picasso's *Harlequin musician*: Mapping and identification of artist materials in situ. *Appl. Spectrosc.* **64**, 584–594 (2010).
5. C. Cucci, J. K. Delaney, M. Picollo, Reflectance hyperspectral imaging for investigation of works of art: Old master paintings and illuminated manuscripts. *Acc. Chem. Res.* **49**, 2070–2079 (2016).
6. T. Vitorino, A. Casini, C. Cucci, M. J. Melo, M. Picollo, L. Stefani, Non-invasive identification of traditional red lake pigments in fourteenth to sixteenth centuries paintings through the use of hyperspectral imaging technique. *Appl. Phys. A* **121**, 891–901 (2015).
7. F. Casadio, L. Toniolo, The analysis of polychrome works of art: 40 years of infrared spectroscopic investigations. *J. Cult. Herit.* **2**, 71–78 (2001).
8. M. Spring, C. Ricci, D. A. Peggie, S. G. Kazarian, ATR-FTIR imaging for the analysis of organic materials in paint cross sections: Case studies on paint samples from the National Gallery, London. *Anal. Bioanal. Chem.* **392**, 37–45 (2008).
9. G. Sciutto, P. Oliveri, S. Prati, E. Catelli, I. Bonacini, R. Mazzeo, A multivariate methodological workflow for the analysis of FTIR chemical mapping applied on historic paint stratigraphies. *Int. J. Anal. Chem.* **2017**, 4938145 (2017).
10. C. Miliani, F. Rosi, A. Daveri, B. G. Brunetti, Reflection infrared spectroscopy for the non-invasive in situ study of artists' pigments. *Appl. Phys. A* **106**, 295–307 (2012).
11. F. Rosi, C. Miliani, R. Braun, R. Harig, D. Sali, B. G. Brunetti, A. Sgamellotti, Noninvasive analysis of paintings by mid-infrared hyperspectral imaging. *Angew. Chem. Int. Ed.* **52**, 5258–5261 (2013).
12. F. Rosi, A. Daveri, P. Moretti, B. G. Brunetti, C. Miliani, Interpretation of mid and near-infrared reflection properties of synthetic polymer paints for the non-invasive assessment of binding media in twentieth-century pictorial artworks. *Microchem. J.* **124**, 898–908 (2016).
13. F. Gabrieli, K. A. Dooley, J. G. Zeibel, J. D. Howe, J. K. Delaney, Standoff mid-infrared emissive imaging spectroscopy for identification and mapping of materials in polychrome objects. *Angew. Chem. Int. Ed.* **57**, 7341–7345 (2018).
14. K. A. Dooley, D. M. Conover, L. D. Glinsman, J. K. Delaney, Complementary standoff chemical imaging to map and identify artist materials in an early Italian Renaissance panel painting. *Angew. Chem. Int. Ed.* **126**, 13995–13999 (2014).
15. S. Legrand, M. Alfeld, F. Vanmeert, W. De Nolf, K. Janssens, Macroscopic Fourier transform infrared scanning in reflection mode (MA-rFTIR), a new tool for chemical imaging of cultural heritage artefacts in the mid-infrared range. *Analyst* **139**, 2489–2498 (2014).
16. D. M. Conover, "Fusion of reflectance and x-ray fluorescence imaging spectroscopy data for the improved identification of artists' materials," thesis, The George Washington University (2015).
17. K. A. Dooley, J. Coddington, J. Krueger, D. M. Conover, M. Loew, J. K. Delaney, Standoff chemical imaging finds evidence for Jackson Pollock's selective use of alkyd and oil binding media in a famous 'drip' painting. *Anal. Methods* **9**, 28–37 (2017).
18. M. Thoury, J. K. Delaney, E. R. de la Rie, M. Palmer, K. Morales, J. Krueger, Near-infrared luminescence of cadmium pigments: In situ identification and mapping in paintings. *Appl. Spectrosc.* **65**, 939–951 (2011).
19. P. Ricciardi, J. K. Delaney, M. Facini, L. D. Glinsman, Use of imaging spectroscopy and in situ analytical methods for the characterization of the materials and techniques of 15th century illuminated manuscripts. *J. Am. Inst. Conserv.* **52**, 13–29 (2013).

20. P. Ricciardi, J. K. Delaney, M. Facini, J. G. Zeibel, M. Picollo, S. Lomax, M. Loew, Near infrared reflectance imaging spectroscopy to map paint binders in situ on illuminated manuscripts. *Angew. Chem. Int. Ed.* **51**, 5607–5610 (2012).
21. P. Ricciardi, M. Facini, J. K. Delaney, Painting and illumination in early Renaissance Florence: The techniques of Lorenzo Monaco and his workshop, in *The Renaissance Workshop*, D. Saunders, M. Spring, A. Meek, Eds. (The British Museum, 2013), pp. 1–9.
22. C. Invernizzi, T. Rovetta, M. Licchelli, M. Malagodi, Mid and near-infrared reflection spectral database of natural organic materials in the cultural heritage field. *Int. J. Anal. Chem.* **2018**, 7823248 (2018).
23. C. Miliani, A. Daveri, B. G. Brunetti, A. Sgamellotti, CO_2 entrapment in natural ultramarine blue. *Chem. Phys. Lett.* **466**, 148–151 (2008).
24. G. D. Smith, R. J. Klinshaw II, The presence of trapped carbon dioxide in lapis lazuli and its potential use in geo-sourcing natural ultramarine pigment. *J. Cult. Herit.* **10**, 415–421 (2009).
25. J. Kirby, M. Spring, C. Higgitt, The technology of red lake pigment manufacture: Study of the dyestuff substrate. *Natl. Gallery Tech. Bull.* **26**, 71–87 (2005).
26. C. Bisulca, M. Picollo, M. Bacci, D. Kunzelman, UV-Vis-NIR reflectance spectroscopy of red lakes in paintings, in *9th International Conference on Non-Destructive Testing of Art* (2008), pp. 1–8.
27. C. Clementi, B. Dohert, P. L. Gentili, C. Miliani, A. Romani, B. G. Brunetti, A. Sgamellotti, Vibrational and electronic properties of painting lakes. *Appl. Phys. A* **92**, 25–33 (2008).
28. J. K. Delaney, K. A. Dooley, M. Facini, F. Gabrieli, Mapping and identification of the pigments used in two illuminations from the Laudario of Sant'Agnese attributed to the Master of the Dominican Effigies, in *Manuscripts in the Making: Art and Science Volume II*, S. Panayotova, P. Ricciardi, Eds. (Brepols Publishers, 2018).
29. E. Martin, M. Eveno, Contribution to the study of old green copper pigments in easel paintings, in *3rd International Conference on Nondestructive Testing, Microanalytical Methods and Environment Evaluation for Study and Conservation of Works of Art* (1992), pp. 779–792.
30. J. Dunkerton, A. Roy, The materials of a group of late fifteenth-century Florentine panel paintings. *Natl. Gallery Tech. Bull.* **17**, 20–31 (1996).
31. B. H. Berrie, M. Leona, R. McLaughlin, Unusual pigments found in a painting by Giotto (c. 1266-1337) reveal diversity of materials used by medieval artists. *Herit. Sci.* **4**, 1 (2016).
32. L. M. Smieska, R. Mullett, L. Ferri, A. R. Woll, Trace elements in natural azurite pigments found in illuminated manuscript leaves investigated by synchrotron X-ray fluorescence and diffraction mapping. *Appl. Phys. A* **123**, 484 (2017).
33. F. Vanmeert, E. Hendriks, G. Van der Snickt, L. Monico, J. Dik, K. Janssens, Back Cover: Chemical mapping by macroscopic x-ray powder diffraction (MA-XRPD) of Van Gogh's Sunflowers: Identification of areas with higher degradation risk (Angew. Chem. Int. Ed. 25/2018). *Angew. Chem. Int. Ed.* **57**, 7534 (2018).
34. R. L. Frost, W. N. Martens, L. Rintoul, E. Mahmutagic, J. T. Kloprogge, Raman spectroscopic study of azurite and malachite at 298 and 77 K. *J. Raman Spectrosc.* **33**, 252–259 (2002).
35. R. L. Frost, D. L. Wain, W. N. Martens, B. J. Reddy, Vibrational spectroscopy of selected minerals of the rosasite group. *Spectrochim. Acta A Mol. Biomol. Spectrosc.* **66**, 1068–1074 (2007).
36. M. C. Hales, R. L. Frost, Synthesis and vibrational spectroscopic characterisation of synthetic hydrozincite and smithsonite. *Polyhedron* **26**, 4955–4962 (2007).
37. R. L. Frost, A. Lópes, R. Scholz, Y. Xi, Infrared and Raman spectroscopic characterization of the arsenate mineral ceruleite $Cu_2Al_7(AsO_4)_4(OH)_{13}{\cdot}11.5(H_2O)$. *Spectrochim. Acta A Mol. Biomol. Spectrosc.* **116**, 518–523 (2013).
38. M. Alfeld, J. V. Pedroso, M. van Eikema Hommes, G. Van der Snickt, G. Tauber, J. Blaas, M. Haschke, K. Erler, J. Dik, K. Janssens, A mobile instrument for in situ scanning macro-XRF investigation of historical paintings. *J. Anal. At. Spectrom* **28**, 760–767 (2013).
39. J. K. Delaney, D. M. Conover, K. A. Dooley, L. D. Glinsman, K. Janssens, M. Loew, Integrated x-ray fluorescence and diffuse visible-to-near-infrared reflectance scanner for standoff elemental and molecular spectroscopic imaging of paints and works on paper. *Herit. Sci.* **6**, 31 (2018).

Acknowledgments: We thank J. E. Post, National Gem and Mineral Collection, Smithsonian Institution, for the use of the mixite samples. We thank painting conservators D. Anchin, K. Raynor, and J. Hickey for making the mock-up painting and G. Bent, Washington and Lee University, for the art historical comments. We also thank F. Rosi and C. Miliani for sharing knowledge on the interpretation of the mid-IR spectra. **Funding:** This research was supported by the Samuel H. Kress Foundation, the Andrew W. Mellon Foundation, and the National Gallery of Art in Washington, DC. **Author contributions:** F.G., M.F., and J.K.D. collected the data. F.G. processed the data, and F.G., J.K.D., and K.A.D. interpreted the results and wrote the paper. **Competing interests:** The authors declare they have no competing interest. **Data and materials availability:** All data needed to evaluate the conclusions in the paper are present in the paper. Additional data related to this paper may be requested from the authors.

Submitted 23 January 2019
Accepted 16 July 2019
Published 23 August 2019
10.1126/sciadv.aaw7794

Citation: F. Gabrieli, K. A. Dooley, M. Facini, J. K. Delaney, Near-UV to mid-IR reflectance imaging spectroscopy of paintings on the macroscale. *Sci. Adv.* **5**, eaaw7794 (2019).